Femtosecond Laser Direct Writing of Polarization-Controllable DBR Fiber Lasers for Harsh Environmental Vibration/Acoustic Sensing

Runxiao Chen, Xizhen Xu, Kuikui Guo, Yihang Wang, Bin Du, Feng Zhu, Ying Wang, Changrui Liao, *Member, IEEE,* Yiping Wang, *Fellow, OSA/Senior Member, IEEE,* and Jun He, *Member, IEEE*

Abstract—Single-frequency distributed Bragg reflector fiber lasers (DBR FLs) are attractive as sensing elements for detecting weak vibration or acoustic signals in extreme environments. However, conventional UV-written DBR FLs operate with two orthogonal polarization modes and can hardly operate in high-temperature environments. Herein, we propose the fabrication of polarization-controllable DBR FLs by using a slit beam shaping femtosecond (fs) laser point-by-point technology. High-quality fiber Bragg grating Fabry-Perot (FBG-FP) cavities with insertion loss as low as 0.2 dB are directly inscribed in Er-doped fibers to create DBR FLs. Both single-polarization and dual-polarization DBR FLs are created by changing the fs laser-induced birefringence using a mechanical slit. In addition, a DBR FL array consisting of eight DBR FLs is also successfully created. Experimental results show that the fabricated DBR FL can withstand a high temperature up to 800 ℃ and the laser linewidth increases from 1.55 kHz to 10.8 kHz as temperature raising from 25 ℃ to 800 ℃. Furthermore, high-temperature vibration sensing at 800 ℃ is realized by using a single-polarization DBR FL, achieving an acceleration sensitivity of 0.319 rad/(m/s^2). Moreover, a dual-polarization DBR FL is served as an ultrasonic sensor, realizing the ultrasonic non-destructive evaluation (NDE) in a 7075-aluminum plate.

***Index Terms*—Distributed Bragg reflector fiber lasers (DBR FLs), Femtosecond laser materials processing, Extreme environment sensing[1].**

I. Introduction

Extreme physical conditions such as high temperature, ionizing radiation and high pressure occur in the fields of aerospace industry, nuclear plants, oil and gas industry and others. For example, along with other extreme conditions, harsh temperature takes place in the gas turbine (~650 ℃), various nuclear reactors from light water to high-temperature reactors (300-1000 ℃), and hydrothermal fluids in deep geothermal wells (~600 ℃) [1-3]. Importantly, it is necessary to continuous and real-time monitor structures for fault or damage, ensuring their safe operation or issuing early warnings for predictive maintenance. However, structure health monitoring by detecting weak signals like vibration and acoustic in extreme environments remain as a challenge. For decades, the commonly used detection elements were piezoelectric transducers (PZTs), whereas they suffered from corrosion, electromagnetic interference, thermal degradation, and limited multiplexing capacity, hindering their practical use in harsh environments [4]. In recent years, fiber-optic sensors emerge as attractive sensing elements due to their distinct advantages such as small footprint, corrosion resistance, electromagnetic interference immunity, high temperature resistance and large-scale multiplexing capability, which are promising for applications in extreme environmental conditions [5-7].

Single-frequency distributed Bragg reflector fiber laser (DBR FL) has attracted considerable interests in the field of fiber-optic sensors. Such a device exhibits great advantages of compactness, narrow linewidth, low noise, and high signal-to-noise ratio (SNR), and hence can reach an ultrahigh sensitivity in detecting weak signals [8, 9]. A typical DBR FL cavity consists of a pair of narrowband fiber Bragg gratings (FBGs), i.e., FBG Fabry-Perot (FBG-FP) cavity, within a short section of rare-earth-doped fiber. Generally, DBR FLs written in non-polarization-maintaining active fiber by ultraviolet (UV) irradiation operate with two orthogonal polarization modes due to the intrinsic and UV-induced birefringence [10, 11]. The dual-polarization DBR FL offers a beat signal in the radio-frequency (RF) domain, making it an attractive high-sensitivity sensing element based on the optical heterodyne detection [12]. Measurement of various signals such as temperature, axial strain, lateral force, bending, and ultrasonic wave has been demonstrated based on the polarimetric heterodyning sensors [13-18]. Conversely, for fiber sensing systems based on phase detection with imbalanced interferometers, the power exchange between

Manuscript received 31 May 2024; revised 16 August 2024; accepted 25 August 2024. Date of publication XXXX, 2024. Date of current version XXXX, 2024.

This research is supported by National Natural Science Foundation of China (NSFC) (62222510, 62375176); National Key Research and Development Program of China (2023YFB3208600); Department of Science and Technology of Guangdong Province (2022B1515120050); Shenzhen Key Laboratory of Ultra-fast Laser Micro/Nano Manufacturing (ZDSYS20220606100405013). *(Corresponding author: Yiping Wang).*

Runxiao Chen, Xizhen Xu, Yihang Wang, Bin Du, Feng Zhu, Ying Wang, Changrui Liao, Yiping Wang and Jun He are with Shenzhen Key Laboratory of Ultrafast Laser Micro/Nano Manufacturing, Guangdong and Hong Kong Joint Research Centre for Optical Fibre Sensors, Shenzhen University, Shenzhen 518060, China, and also with the State Key Laboratory of Radio Frequency Heterogeneous Integration, Key Laboratory of Optoelectronic Devices and Systems of Ministry of Education/Guangdong Province, College of Physics and Optoelectronic Engineering, Shenzhen University, Shenzhen 518060, China. Yiping Wang is also with the Guangdong Laboratory of Artificial Intelligence and Digital Economy (SZ), Shenzhen 518107, China. (e-mail: 2060453041@email.szu.edu.cn; xizhenxu@szu.edu.cn; 2466742528@qq.com; dubin2016@email.szu.edu.cn; zhufeng@szu.edu.cn; yingwang@szu.edu.cn; cliao@szu.edu.cn, ypwang@szu.edu.cn, hejun07@szu.edu.cn)

Kuikui Guo is with School of Electrical Engineering and Intelligentization, Dongguan University of Technology, Dongguan 523808, China. (2022090@dgut.edu.cn)

two polarization modes is undesirable because it will lead to signal fading. To address this challenge, numerous efforts have been dedicated to obtain single-polarization FLs. For example, twisting-induced circular birefringence, stress-induced phase-shift birefringence, injection locking technique, co-pumping configuration with an increasing pump power, and UV-induced permanent birefringent phase-shift have been demonstrated as effective methods to obtain FLs with single-polarization mode [19-23]. Nonetheless, the schemes for achieving single-polarization FLs mentioned above are post-processing methods, which are not straightforward and flexible enough to tailor both single-polarization and dual-polarization FLs.

For sensing in extreme environments, high temperature resistance is a key factor. However, conventional UV-induced DBR-FLs can hardly operate in high temperature above 600 ℃ due to the thermal degradation of FBGs [24-26]. DBR FL based on regenerated FBGs exhibited a higher temperature resistance at 750 ℃, whereas it required a complicated hydrogen loading process to enhance photosensitivity of the fibers [27]. Notably, type II FBGs inscribed by femtosecond laser exhibit excellent high-temperature resistance and long-term stability, acting as good candidates for harsh environmental sensing [28-30]. DBR FL based on type II FBGs were inscribed by using a femtosecond laser phase mask method, presenting a high-temperature resistance of 1000 ℃ [31]. However, since the grating pitches are determined by phase mask, it is difficult to create DBR FLs with various lasing wavelengths by using only one phase mask. Remarkably, the femtosecond laser point-by-point (PbP) technology exhibits great flexibility in fabricating FBGs with various wavelengths by controlling the repetition rate and velocity of fiber movement during inscription process [32, 33]. In 2006, it was reported for the first time the femtosecond PbP technology was employed to inscribe DBR FL, which operated with a single polarization mode based on distinct polarization-dependent grating strength resulted from the fs laser-induced birefringence [34]. However, this PbP DBR FL can only operate at 600 ℃ because low pulse energies were used and type I FBGs were formed in their experiment. Moreover, it is well known that the type II PbP-FBGs with structural changes formed with high pulse energies can withstand temperatures above 1000 ℃ [35]. Nevertheless, PbP-FBGs typically exhibit strong insertion loss (IL) and weak coupling strength, which will decrease the capacity for wavelength division multiplexing [36]. In recent years, novel beam shaping techniques were proposed for fabricating Bragg gratings via mechanical slit, cylindrical lens, non-diffractive beams, filamentation and so on [37-40]. By utilizing a cylindrical lens or filamentation, the cross-section of refractive index modulation (RIM) for PbP-FBGs were extended as planes or lines, thereby favoring an enhancement of the grating strength [41, 42]. However, both methods would inevitably result in considerable grating birefringence due to the asymmetric RIMs, making it challenging to fabricate polarization-controllable DBR FLs using these methods. Remarkably, the slit beam shaping method has successfully yielded high-quality PbP-FBGs that exhibit both high reflectivity and low insertion loss, rendering them ideally suited for use as cavity mirrors in the DBR FLs [43]. Furthermore, the cross-sectional shape of fs laser-induced RIM could be controlled by adjusting the slit width, which can be developed for flexibly tailoring the grating strength and birefringence [44, 45].

In this article, polarization-controllable DBR FLs created by a slit beam shaping femtosecond laser PbP technology is proposed and demonstrated. A mechanical slit is employed to shape the fs laser beam, which can flexibly change the grating strength and the induced birefringence. Both single-polarization and dual-polarization DBR FLs were created by inscribing high-quality FBG-FP cavities with different fs laser-induced birefringence. In addition, a DBR FL array consisting of eight DBR FLs was also successfully created by inscribing FBG-FP cavities with distinct grating periods. Subsequently, high-temperature response of the DBR FL was investigated. It was demonstrated that the fabricated DBR FL can withstand a high temperature up to 800 ℃ and the laser linewidth increases from 1.55 kHz to 10.8 kHz as temperature raising from room temperature to 800 ℃. Furthermore, to the best of our knowledge, we present the first vibration sensing at a high temperature of 800 ℃ using a single-polarization DBR FL, achieving an acceleration sensitivity of 0.319 rad/(m/s^2). Moreover, a dual-polarization DBR FL was utilized as an ultrasonic sensor, realizing the ultrasonic non-destructive evaluation (NDE) of a 7075-aluminum plate by detecting the laser-acoustic surface wave. As a result, the proposed polarization-controllable and high-temperature-resistant DBR FLs exhibit promising potential for structure health monitoring in extreme environments.

II. Device Fabrication and Characterization

A. Working principle

The schematic of the working principle for fabricating polarization-controllable DBR FLs and their sensing mechanisms are illustrated in Fig. 1. A femtosecond laser with a center wavelength of 513 nm, a pulse duration of 290 fs and a repetition rate of 200 kHz was employed [45]. The laser pulses were normally incident on a mechanical slit inserted parallel-oriented to the fiber axis, and then focused into a coating-removed erbium-doped fiber (EDF, Nufern SM-ESF-7/125) by an oil-immersion microscope objective (MO, Leica 100×, NA=1.25). The MO and EDF were immersed in the index-matching oil to minimize the distortions introduced by the curved surface of the fiber. PbP-FBGs could be written by translating the fiber relative to the focal region of laser beam with a constant speed and laser repetition frequency, and hence a DBR FL could be created by inscribing an FBG-FP cavity in the core of an EDF. When a 980 nm pump laser was launched into the FBG-FP cavity, continuous laser output would be emitted as the pump power exceeded the threshold. As the previous study, a strong polarization selective between two orthogonal polarization modes can be achieved when satisfying the condition of $2|\kappa L_x-\kappa L_y|/(\kappa L_x+\kappa L_y)>0.012$, where κL_x and κL_y defined here are the coupling grating strength for x-polarization mode and y-polarization mode, respectively [46]. Notably, it has been proven that single polarization mode was selected for distributed feedback FL

written by the femtosecond laser PbP technology, which is due to the significant polarization-dependent grating strengths resulting from the birefringence inscribed by the femtosecond laser [47]. For the detection of dynamic signal like axial vibration, the sensing mechanism for the single-polarization DBR FL is based on the strain-induced drift of the operation wavelength through the photoelastic effect [48]. Taking advantage of an interferometer with an imbalanced length of d, a slight variation of the wavelength drift ($\Delta\lambda$) can be translated into a detectable optical phase difference ($\Delta\varphi$), i.e., $\Delta\varphi=2\pi nd\Delta\lambda/\lambda^2$, where n represents the effective refractive index [49]. Therefore, a dynamic strain applied to the single-polarization DBR FLs can be detected by monitoring the variation of optical phase, which could be decoded by phase demodulation algorithms. Meanwhile, it demonstrates that DBR FLs exhibit a higher sensitivity compared to FBGs, thus offering a distinct advantage for detecting weak signals.

For the fabrication of DBR FLs operating with two orthogonal polarization modes, a reduced polarization-dependent grating strength is necessary. Herein, a beam shaping method based on a mechanical slit was employed to create dual-polarization DBR FLs. Note that the focal beam waist (ω) is dependent on the incident beam waist (W), focal length (f), and laser wavelength (λ), i.e., $\omega=f\lambda/\pi W$ [50]. Therefore, with appropriate pulse energy, the RIM area of DBR FLs can be effectively enlarged by reducing W that determined by the slit width (w), as shown in the schematic fiber core cross-section of the reshaping RIMs in Fig. 1. As the grating birefringence is highly dependent on the ellipticity of RIMs, DBR FLs operating with two orthogonal polarization modes can be created in a way of reducing the introduced birefringence by shaping the RIMs with a smaller ellipticity in cross-section [51]. For the dual-polarization DBR FL, a beat frequency $\Delta f=|f_x-f_y|=cB/n\lambda$ arises in the RF region due to the slightly different operation frequencies f_x and f_y for the two eigenpolarization modes, where $B=|n_x-n_y|$ denotes the birefringence difference. When the laser cavity is perturbed by a dynamic signal like ultrasonic wave, the fiber will be compressed and stretched in the two orthogonal directions due to the radial pressure, and hence the beat frequency is modulated resulting from the induced birefringence change in the resonant cavity [17]. For the reconstruction of the modulated signal, the I/Q demodulation method can be employed [52].

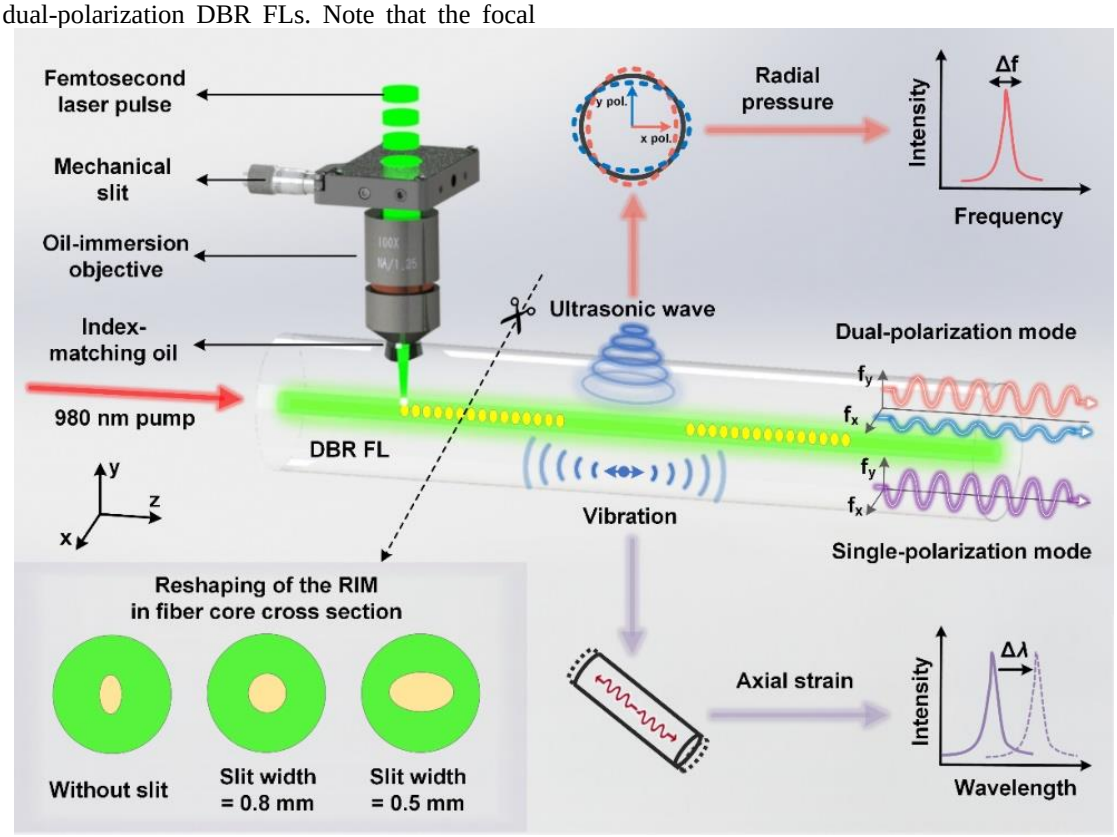

Fig. 1. Working principle for fabricating polarization-controllable DBR FLs and their sensing mechanisms. Schematic diagram shows the femtosecond laser direct-writing of polarization-controllable DBR FLs using a slit beam shaping technique and the sensing mechanisms of vibration and ultrasonic wave for single- and dual-polarization DBR FLs, respectively.

B. Fabrication of DBR FLs

In the experiment, three FBG-FP cavities S1-S3 were created in EDFs by the slit beam shaping femtosecond laser PbP technology. The sample S1 was inscribed without slit beam shaping while S2 and S3 were inscribed with a slit width of 0.85 mm and 0.5 mm, respectively. Femtosecond laser beams with on-target single pulse energy of 14 nJ, 27 nJ and 38 nJ were tightly focused into the EDF core for inscribing S1, S2 and S3, respectively. All the FP-FBG cavities consists of two uniform first-order FBGs with a grating period of 0.535 μm and a grating length of 15 mm. The interval between two FBGs was 2 mm to construct single-frequency DBR FLs. To obtain the cross-sectional images, a fiber cleaver was employed to transversally

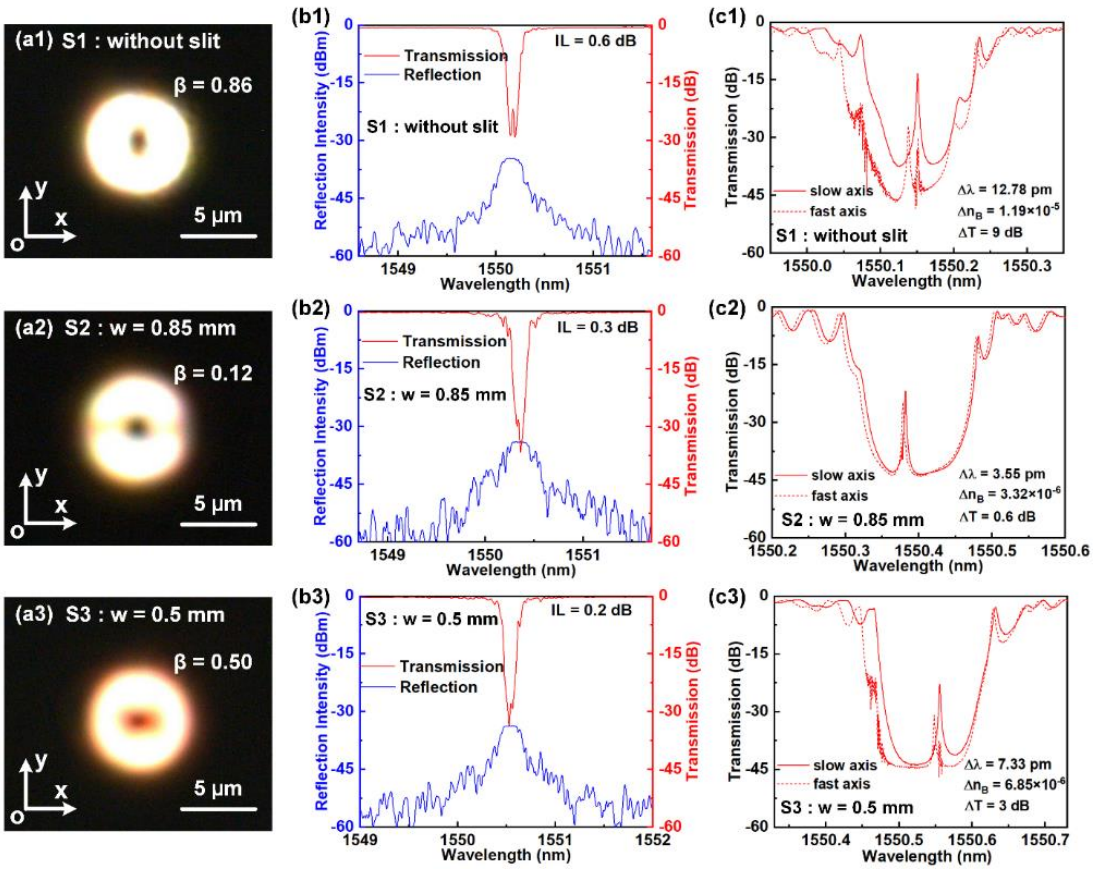

Fig. 2. Three DBR FLs inscribed by femtosecond laser PbP technology without slit beam shaping (i.e., S1), with slit width of 0.85 mm (i.e., S2) and 0.5 mm (i.e., S3). (a) Cross-sectional-view microscope images. (b) Transmission and reflection spectra. (c) Transmission spectra measured for the slow (solid lines) and fast (dashed lines) polarization axes.

cleave the grating region and then the fiber cross-sections were observed and captured on a microscope (Leica DM2700MH). The cross-sectional-views of S1-S3 are shown in Figs. 2 (a1) -(a3), respectively. Apparently, the width on the x axis (w_x) of the RIM areas increases while the height on the y axis (h) almost remains unchanged after introducing a slit, and this tendency continues as the slit width decreases. In addition, the ellipticity (β) of the RIM can be calculated by their height and width as $\beta=|h/w_x-1|$. Among the three samples, the RIM of S1 presents the maximum ellipticity of $\beta1$=0.86 while S2 exhibits as a near-circular pattern with the minimum ellipticity of $\beta2$=0.12 and S3 has a middle ellipticity of $\beta3$=0.50. As a result, the ellipticity of the RIM are effectively controlled by adjusting the slit width.

During the fabrication process, the transmission and reflection spectra of DBR FLs were real-time monitored by using a broadband source (BBS, Fiberlake) within a wavelength range of 1520-1580 nm and an optical spectrum analyzer (OSA, Yokogawa AQ6370C) with a resolution of 0.02 nm. The transmission and reflection spectra of S1-S3 are exhibited in Figs. 2 (b1) -(b3), obtained when the grating inscription process was finished. We can observe from the transmission spectra of S1-S3 that there is one narrow resonant peak within the transmission band, corresponding to a single longitudinal mode of the DBR FL. The transmission attenuation of S1-S3 is more than -30 dB and the out-of-band loss is 0.6 dB, 0.3 dB and 0.2 dB, respectively. The reduced IL with slit beam shaping may result from the reduction of laser peak intensity gradient to suppress the light scattering [52]. Limited by the resolution of the OSA and the output power of the BBS, the actual resonant attenuation of the transmission band and narrow peak could not be measured accurately. As a result, high-quality FP-FBG cavities with high reflectivity of more than 99.9% and insertion loss as low as 0.2 dB have been created attributing to the slit beam shaping.

In addition, polarization-resolved transmission spectra of S1-S3 were measured by a commercial polarization analysis system, which consists of a tunable laser (Keysight N7776C), a polarization synthesizer (Keysight N7788C) and an optical power meter (Keysight N7744C). The wavelength resolution of the system is 0.15 pm. As shown in the spectra measured for the fast and slow polarization axes in Figs. 2 (c1) -(c3), the wavelength detuning $\Delta\lambda$ of the FP-FBG cavities S1-S3 is 12.78 pm, 3.55 pm and 7.33 pm, respectively. The corresponding induced birefringence Δn_B for S1-S3 is 1.19×10^{-5}, 3.32×10^{-6} and 6.85×10^{-6} calculated by $\Delta n_B=\Delta\lambda/2\Lambda$, where Λ is the grating period. Notably, Δn_B exhibits a strong correlation with the ellipticity of the induced RIM, demonstrating a consistent trend with the previously reported calculations conducted by Jovanovic [44]. Compared to S1 and S3 with a larger ellipticity of the RIM, the induced birefringence of S2 with a near-circular RIM is effectively reduced, which is comparable to a magnitude of the conventional UV-inscribed DBR FLs [53]. It is known from the previous study that the slow axis of the PbP-FBGs corresponds to light polarized parallel to the long axis of the elliptical RIM [44]. Therefore, this indicates that the slow polarization axis for S1 is parallel to y axis in Fig. 2 (a1), while slow polarization axis for S2 and S3 corresponds to the x axis in Figs. 2 (a2) -(a3). Moreover, the polarization-dependent grating strength ΔT (i.e., the difference of the grating strength for different polarization

axes) for S1-S3 is 9 dB, 0.6 dB and 3 dB, respectively. It presents that the polarization-dependent grating strength for DBR FLs can be effectively adjusted by controlling the induced birefringence via reshaping the RIM cross-section.

Subsequently, the DBR FLs were pumped by a 980 nm laser diode through a 980/1550 nm wavelength division multiplexer (WDM). The backward output laser from the resonant cavity was transmitted through the 1550 nm port of the WDM and recorded by an optical power meter. To prevent the cavity from reflective light perturbance, an isolator was connected between the WDM and the power meter. The forward residual pump power was measured by another power meter. Fig. 3 (a) presents the evolution of output power and corresponding pump power for the DBR FLs S1-S3. It was found that the lasing threshold power for S1-S3 is 9 mW, 11 mW, and 14 mW, respectively. As the pump power increases, the output power presents an increasing trend, offering slope efficiencies for S1-S3 of 0.13%, 0.17% and 0.36% calculated by linear fits. Moreover, the output lasing spectra of the DBR FLs at a pump power of 100 mW are shown in Fig. 3 (b), presenting a lasing wavelength for S1-S3 of 1550.156 nm, 1550.368 nm, and 1550.564 nm with corresponding signal noise ratio (SNR) and output power of 59 dB, 61 dB, 63 dB and 110 μW, 145 μW and 298 μW, respectively. It is worth mentioning that S3 exhibits the highest output efficiency among them while S1 shows the lowest efficiency. Since the reflectivity and the length of grating cavities for the three DBR FLs are similar, the difference of output efficiency among them probably due to the different intra-cavity loss. Therefore, the increasing efficiency for DBR FLs fabricated with slit beam shaping may result from the reduced insertion loss, as mentioned in the section 2.2.

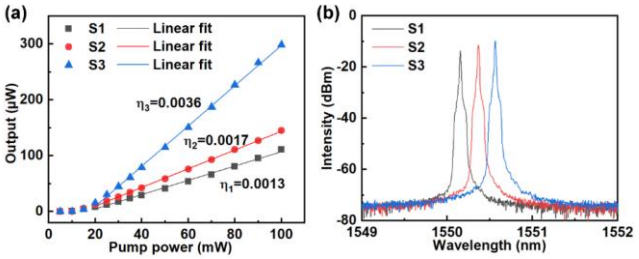

Fig. 3. Laser output measurement of the three inscribed DBR FLs S1-S3. (a) Laser output power versus input pump power. (b) Output lasing spectra at pump power of 100 mW.

C. Wavelength-division-multiplexed DBR FL arrays

We have also demonstrated the flexibility in fabricating wavelength-division-multiplexed DBR FL array by using the proposed method. Here, each FBG-FP cavity was fabricated by inscribing two 5 mm-long first-order FBG with an interval of 2 mm in the EDF. As shown in Fig. 4 (a), a DBR FL array consisting of eight DBR FLs with different lasing wavelengths ranged from 1536.6 to 1550.5 nm at a ~1.8 nm interval was successfully created by tuning the grating period in each FBG-FP cavity. The DBR FL intensity in the array decreases when the pump light incidents from the DBR FL 1 side. This may result from the spontaneous radiation of erbium ions and successive absorption of pump power in the array. Moreover, the DBR FL 5 has the lowest SNR of 35.4 dB, which may probably be introduced by its relatively large insertion loss. Figure 4 (b) shows the photograph of the lasing DBR FL array at a pump power of 100 mW. Visible green and red light from

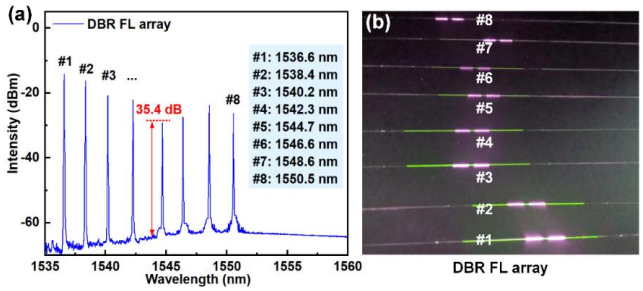

Fig. 4. Wavelength-division-multiplexed DBR FL array consisting of eight DBR FLs created by the slit beam shaping femtosecond laser PbP technology. (a) Output spectrum and (b) photograph of the DBR FL array.

the EDFs can be observed, where the green light results from the fluorescence effect, while red light is due to scattering of the grating regions. The difference of the green fluorescence could be attributed to variations in pump absorption. As a result, the DBR FL array can provide a new approach to wavelength division multiplexing for a large number of fiber laser sensors.

D. Polarization mode characteristics

The polarization mode characteristics of the DBR FLs S1-S3 were experimentally investigated using a scanning Fabry-Perot interferometer (SFPI, Thorlabs SA200-12B) with a free spectral range (FSR) of 1.5 GHz and a resolution of 7.5 MHz. To reduce the external perturbance to polarization states, we ensure that the SMFs which connects the two ends of the laser is straight but not curved and twisty. During the experiment, the pump power was remained constant as 100 mW for SFPI spectra measurement of S1-S3. As illustrated in red and green curves of Fig. 5 (a), two stable peaks can be observed in a scanning period, indicating that the DBR FLs S1 and S3 were operated with a single polarization mode. However, two sets of stable peaks with different amplitude were simultaneously detected in a scanning period, as shown in the blue curves of Fig. 5 (a). This means that two orthogonal polarization modes without intercoupling were operated for the DBR FL S2. The interval of the eigenfrequencies for two polarizations can be estimated as 446 MHz by measuring the time interval between the two adjacent peaks. In addition, we have further measured the RF signal spectrum of DBR FLs S1-S3 using a frequency spectrum analyzer (FSA, Keysight N9030B) and a high-speed photodetector (PD, Newport 1592). Figure 5 (b) exhibits The RF signals of S1-S3 from 0 to 1.8 GHz with a resolution of 1 kHz. It can be observed from the blue curve that a beat peak with a SNR of ~38 dB is located at 446 MHz, in accordance with the value estimated from the SFPI spectrum. However, beat peak is absent for S1 and S3 since they operate with a single polarization mode due to the significant polarization-dependent grating strength induced

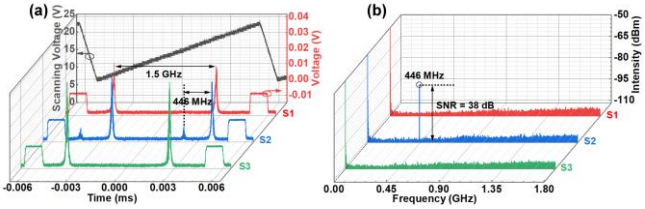

Fig. 5. Polarization mode characteristics for DBR FLs S1-S3, indicating S1 and S3 operate with a single polarization mode and S2 operates in dual-polarization mode manifested by (a) scanning FPI spectra and (b) RF spectra of beat signal.

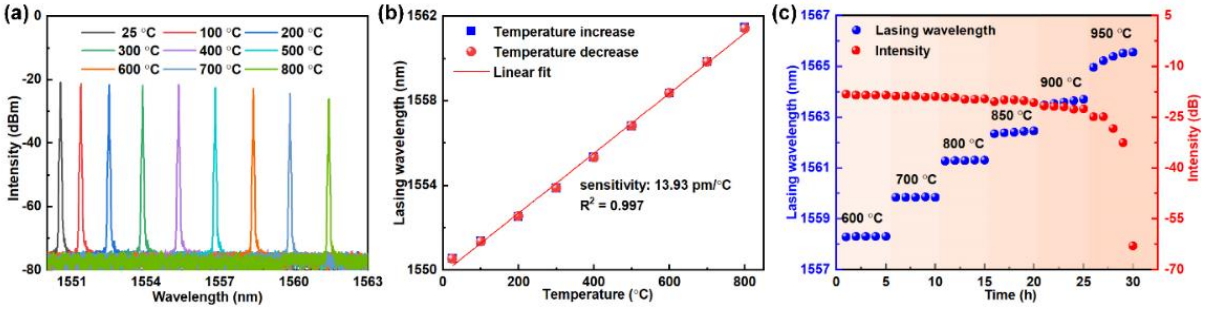

Fig. 6. High temperature resistance characteristics of the DBR FL. (a) Lasing spectrum evolution of the DBR FL during heating process. (b) Lasing wavelength as functions of temperature increase and decrease. (c) Long-term stability of lasing wavelength and output power of DBR FL at high temperatures.

by femtosecond laser inscription. Therefore, both single-polarization and dual-polarization DBR FLs is fabricated by tuning the birefringence and thus the polarization-dependent grating strength using the slit beam shaping.

E. High temperature characteristics

Furthermore, we have studied the high temperature resistance of the DBR FL using a tube furnace (Carbolite, Gero HTRH). The DBR FL was placed in the center of furnace while the temperature was risen from room temperature (25 ℃) to 800 ℃. At each temperature, the test duration was set at 10 minutes to stabilize the temperature in the furnace for obtaining a stable lasing spectrum. During the test, the pump power remained unchanged at 50 mW. The evolution of lasing output spectrum with temperature is shown in Fig. 6 (a). The lasing wavelength exhibits a 'red' shift with an increasing temperature. It is worth noting that no mode hopping was observed during the heating process. As shown in Fig. 6 (b), linear fits were performed to the measured data of temperature increase and decrease, presenting almost overlap curves with a nearly identical sensitivity of 13.93 pm/℃. Moreover, the long-term stability of the DBR FL was tested at increasing high temperatures from 600 ℃ to 950 ℃. At each temperature, the lasing wavelength and peak intensity were recorded in 5 hours with an interval of 1 hour. The results are shown in Fig. 6 (c), in which the laser wavelength and intensity are quite stable below 800 ℃. When the temperature is higher than 800 ℃, the laser wavelength occurs to be unstable and the laser intensity decreases. And eventually, the DBR FL was not lasing at 950 ℃. After this extreme operating temperature, the DBR-FL could not recover to its original operation and response due to the spectral degeneration of the gratings.

The linewidth characteristics of DBR FL was also investigated by using a delayed self-heterodyne (DSH) method [53]. Note that a 50 km single-mode fiber delay line and an acousto-optic modulator (AOM) with a frequency shift of 70 MHz were used in the DSH system. The linewidth of the DBR FL can be estimated by a calculation to half of -3 dB bandwidth of the beat peak. The heterodyne signals obtained from the electrical spectra at 25 ℃ and 800 ℃ are exhibited in Figs. 7 (a) and (b), respectively. Lorentz fits (red curves) of the measured data (blue curves) were carried out, indicating a laser linewidth of 1.55 kHz and 10.8 kHz for DBR FL at 25 ℃ and 800 ℃, respectively. Note that the linewidth of DBR FL was broadened at high temperature, which may result from the increased amplified spontaneous emission (ASE) at high temperature [54]. Nonetheless, the DBR FL still exhibits a relatively remarkable linewidth at high temperature of 800 ℃, which emerges to be a good candidate for sensing in high-temperature environments.

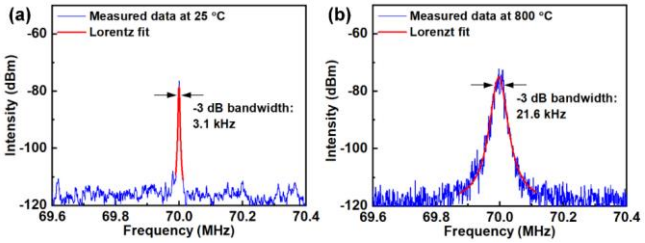

Fig. 7. Linewidth characteristics of the DBR FL measured by a delayed self-heterodyne method at (a) 25 ℃ and (b) 800 ℃. The estimated linewidth of the DBR FL is 1.55 kHz and 10.8 kHz at 25 ℃ and 800 ℃, respectively.

III. SENSING APPLICATIONS

A. High-temperature vibration sensing based on a single-polarization DBR FL

Taking advantage of the high-temperature performance of the DBR FLs, vibration sensing experiments at a high temperature of 800 ℃ were carried out using a single-polarization DBR FL. To decode the vibration signal, a phase demodulation scheme based on a 3×3 coupler interferometer was adopted, as shown in Fig. 8 (a). The signal light from the DBR FL was transmitted into a Michelson interferometer with an imbalanced fiber length of 5 m. Two Faraday rotating mirrors (FRMs) were employed to achieve an optimum visibility of interference fringe and suppress the polarization-induced fading. The interference beam was then received by three PIN PDs and converted into electric signal. Afterwards, the outputs from the PDs were sampled by an analog-to-digital (AD) converter (NI 9215) with a sampling rate of 100 kS/s and transmitted to a personal computer (PC) to perform an arctangent algorithm. In the vibration sensing experiment, the DBR FL was positioned in the center of a tube furnace with one end fixed on the vibration exciter while the other end fixed on a breadboard by epoxy, as illustrated in the schematic for the test in Fig. 8 (b). The DBR FL in the furnace could be visualized by the scattering red light due to the fs laser-induced RIMs when a visible red light was coupled into the fiber, as shown in Fig. 8 (c). During the test, vibration signal with various frequency and amplitude could be generated by the vibration exciter driven by a signal generator. Meanwhile, the actual acceleration applied to exciter was calibrated by a commercial accelerometer (Bruel & Kjaer 8305) mounted on the exciter.

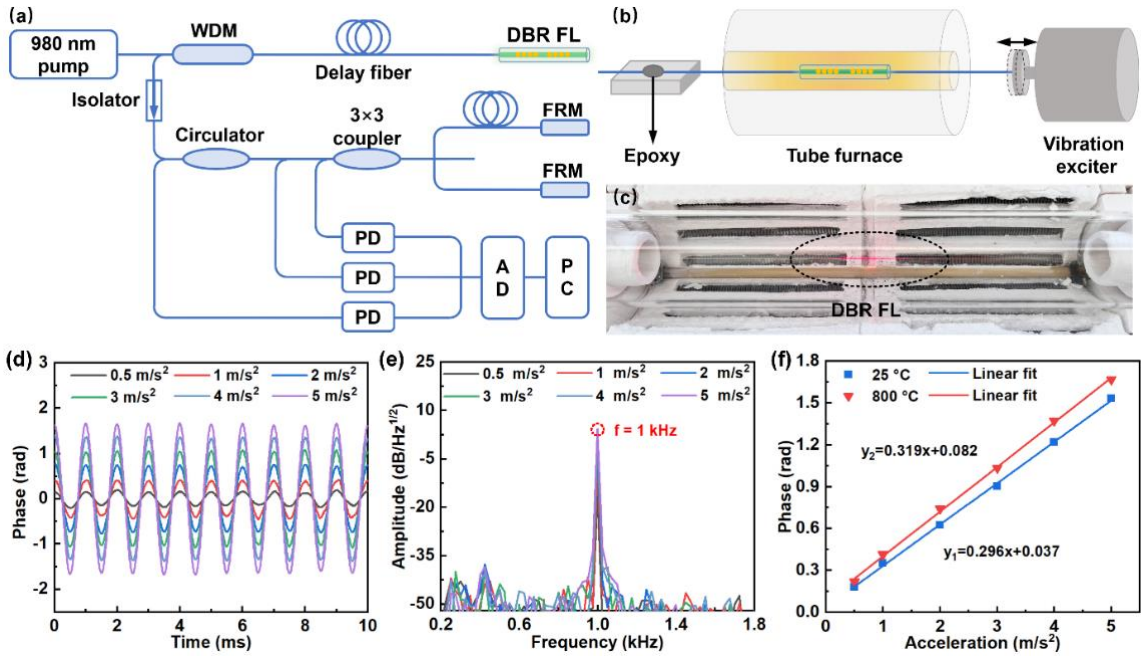

Fig. 8. High-temperature vibration sensing experiments using the single-polarization DBR FL S1. (a) Schematic diagram of the DBR FL sensing system based on a 3×3 coupler interferometer. (b) Schematic diagram of the experimental setup for vibration sensing at high temperature. (c) The DBR FL in the tube furnace. Visible red light is derived from the scattering of the grating region. (d) Acceleration response of the DBR FL at 800 ℃. (e) Frequency spectra of the acceleration response at 800 ℃. (f) Linear responses of the phase amplitude versus acceleration at 25 ℃ and 800 ℃, respectively.

Acceleration response of the DBR FL at 800 ℃ was investigated by applying a series of sinusoidal vibration signals with various accelerations of 0.5, 1, 2, 3, 4 and 5 m/s^2. During the test, the vibration frequency remained constant as 1 kHz. The vibration information was obtained by determining the phase variation in the time domain, as shown in Fig. 8 (d). We can observe that the waveforms of the retrieved curves are standard sinusoidal waves, indicating that the DBR FL responded well to the applied signals. In addition, the corresponding spectra of the retrieved results in the frequency domain were obtained by performing a Fast Fourier Transform (FFT) on the time-domain signals. As illustrated in Fig. 8 (e), it can be clearly observed the resonant peaks are located at 1 kHz, in accordance with the applied frequency. Moreover, the amplitude of the phase is proportional to the applied accelerations, achieving an acceleration sensitivity of 0.319 rad/(m/s^2) at high temperature of 800 ℃, as exhibited in the red curve in Fig. 8 (f). An additional measurement of acceleration response at room temperature of 25 ℃ was carried out, presenting a sensitivity of 0.296 rad/(m/s^2) calculated by performing a linear fit to the blue data in Fig. 8 (f). The increasing acceleration sensitivity at higher temperature may result from the decrease of the stress-optic coefficient [55]. As a result, it turns out that high-temperature vibration sensing at 800 ℃ was achieved by using a single-polarization DBR FL.

B. Ultrasonic non-destructive evaluation based on a dual-polarization DBR FL

Moreover, we have investigated the capability of the dual-polarization DBR serving as an acoustic detection unit in ultrasonic NDE. Generally, ultrasonic NDE is achieved by acoustic generation and detection on a tested piece and analysis of the reflected or transmitted acoustic signal [56, 57]. For the dual-polarization DBR FL, it is known that the fiber birefringence would be modulated when subjecting to an ultrasonic pressure, leading to a beat frequency variation in the RF region [58]. An I/Q quadrature algorithm can be used for the demodulation of ultrasonic signal in the dual-polarization DBR FL sensor systems, as shown in the schematic diagram in Fig. 9 (a). The laser output is transmitted through a polarization controller (PC) and a polarizer for maximizing the beat signals. Then the laser power is amplified from 0.145 mW to 1 mW by an EDFA and launched to a high-speed PD. Note that a suppression of shot noise from the PD and an improvement to SNR of the beat signal could be achieved with the use of the EDFA [59]. Afterwards, the beat signal is detected by an oscilloscope (Tektronix 3054) with a sampling rate of 2.5 GS/s and sent to a computer for processing. In the demodulation process, the input signal is mixed with two quadrature signals which have the identical frequency as the beat signal but a 90-degree phase offset. After the lowpass filtering, two baseband signals in-phase (I) and quadrature-phase (Q) are used to obtain the phase information of the modulated signal by a calculation of arctan(Q/I). Consequently, the modulated frequency can be reconstructed by taking a derivative to the phase data.

To demonstrate the acoustic detection capability of the dual-polarization DBR FL in ultrasonic NDE, a 7075-aluminum plate with a thickness of 20 mm was used as the device under test (DUT). The schematic of the ultrasonic NDE is shown in Fig. 9 (b). The DBR FL was attached on the surface of the DUT with a nearest to-edge distance (D) of 10 mm. The installation of the DBR FL on the 7075-aluminum plate is exhibited in Fig. 9 (c), in which the visible red light is due to the scattering from the grating region. For the ultrasonic generation, a frequency-quadruple Nd:YAG (Spectra-Physics Lab-170-10) free space laser with a 266 nm central wavelength, 10 Hz repetition rate and 4 ns pulse width was employed. The output laser was focused into a 10 mm long line beam by a cylindrical lens, illuminating on the surface of the DUT to excite ultrasonic waves based on the thermo-acoustic effect. During the test, the source-receiver distance was varied from 4 mm to 16 mm by simultaneously moving the DBR FL and

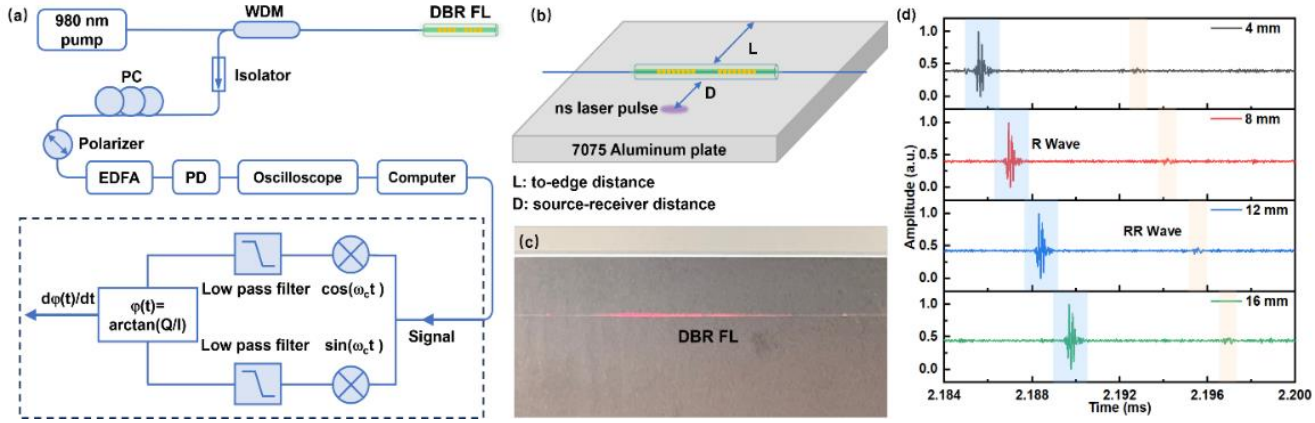

Fig. 9. Experiments of ultrasonic non-destructive evaluation performed on a 7075-aluminum plate using the dual-polarization DBR FL S2 (a) Schematic diagram of the DBR FL sensing system based on the I/Q quadrature demodulation. (b) Schematic diagram of the experimental setup for laser-acoustic detection by a DBR FL on a 7075-aluminum plate. (c) The DBR FL installed on the 7075-aluminum plate. (d) Ultrasonic signals detected by the DBR FL at various source-receiver distances of 4 mm, 8 mm, 12 mm, and 16 mm.

DUT while laser source kept still. In addition, the laser pulse energy for ultrasonic generation was remained constant as 0.5 mJ. The beat frequency of the dual-polarization DBR FL would be modulated as the generated ultrasonic was applied to the laser. By performing a calculation based on the I/Q demodulation method, the ultrasonic signals were reconstructed. As shown in Fig. 9 (d), two different peaks can be observed in the retrieved results in the time domain. The first arriving ultrasound signal is identified as the directly transmitted surface Rayleigh wave (R-wave) while the second is the reflected surface Rayleigh wave (RR-wave) from the edge. By measuring the time difference of arrival (TDOA) for the two peaks, the propagation velocity of the surface Rayleigh wave in 7075-aluminum can be estimated as 2911 m/s, which is close to the actual value of 2850 m/s [60]. In addition, the measured to-edge distance is 10.34 mm by using the TDOA between the adjacent R-waves detected with different source-receiver distance. The slight error of the propagation velocity and to-edge distance may result from the measuring error of the distance and the reading error of TDOA. As a result, ultrasonic NDE is achieved by using the created dual-polarization DBR FL as an ultrasonic detection unit. As a prospect, by replacing the edge of the aluminum plate with a crack, it is promising to realize ultrasonic flaw detection using a dual-polarization DBR FL in the future.

IV. Conclusion

We have proposed and demonstrated a slit beam shaping fs laser point-by-point technology for fabrication of polarization-controllable DBR FLs with high-temperature resistance. Both single-polarization and dual-polarization DBR FLs were created by changing the fs laser-induced birefringence of the FBG Fabry-Perot (FBG-FP) cavity using a slit beam shaping method. High-performance DBR FL was obtained by created a high-quality FBG-FP cavity with a low insertion loss as low as 0.2 dB in a section of Er-doped fiber. In addition, a DBR FL array consisting of eight DBR FLs was also successfully created by inscribing FBG-FP cavities with distinct grating periods. Furthermore, it was demonstrated that the fabricated DBR FL can withstand a high temperature up to 800 ℃ and the laser linewidth increases from 1.55 kHz and 10.8 kHz as temperature raising from 25 ℃ to 800 ℃. Moreover, high-temperature vibration sensing at 800 ℃ was realized by using a single-polarization DBR FL, achieving an acceleration sensitivity of 0.319 rad/(m/s^2). Besides, a dual-polarization DBR FL was successfully applied in ultrasonic NDE in a 7075-aluminum plate. Consequently, this provides a novel approach to fabricate polarization-controllable and high-temperature-resistant DBR FL sensors, which are promising elements for structure health monitoring in extreme environments.

References

[1] H. Xia, D. Byrd, S. Dekate, and B. Lee, "High-Density Fiber Optical Sensor and Instrumentation for Gas Turbine Operation Condition Monitoring," *J. Sens.*, vol. 2013, 2013, Art. no. 206738.
[2] J. Cizek, J. Kalivodova, M. Janecek, J. Strasky, O. Srba, and A. Mackova, "Advanced Structural Materials for Gas-Cooled Fast Reactors-A Review," *Metals*, vol. 11, no. 1, Jan. 2021, Art. no. 76.
[3] E. Bali *et al.*, "Geothermal energy and ore-forming potential of 600 °C mid-ocean-ridge hydrothermal fluids," *Geology*, vol. 48, no. 12, pp. 1221-1225, Dec. 2020.
[4] D. A. van den Ende, W. A. Groen, and S. van der Zwaag, "Development of temperature stable charge based piezoelectric composite quasi-static pressure sensors," *Sens. Actuator A-Phys.*, vol. 163, no. 1, pp. 25-31, Sep. 2010.
[5] M. Wang *et al.*, "Femtosecond laser fabrication of nanograting-based distributed fiber sensors for extreme environmental applications," *Int. J. Extreme Manuf.*, vol. 3, no. 2, Apr. 2021, Art. no. 025401.
[6] S. J. Mihailov, "Femtosecond laser-induced Bragg gratings in silica-based fibers for harsh environment sensing," *APL Photonics*, vol. 8, no. 7, Jul. 2023, Art. no. 071102.
[7] J. He, B. Xu, X. Xu, C. Liao, and Y. Wang, "Review of Femtosecond-Laser-Inscribed Fiber Bragg Gratings: Fabrication Technologies and Sensing Applications," *Photonic Sens.*, vol. 11, no. 2, pp. 203-226, Jun. 2021.
[8] B.-O. Guan, L. Jin, Y. Zhang, and H.-Y. Tam, "Polarimetric Heterodyning Fiber Grating Laser Sensors," *J. Lightwave Technol.*, vol. 30, no. 8, pp. 1097-1112, Apr. 2012.
[9] G. A. Cranch, G. M. H. Flockhart, and C. K. Kirkendall, "Distributed feedback fiber laser strain sensors," *IEEE Sens. J.*, vol. 8, no. 7-8, pp. 1161-1172, Jul.-Aug. 2008.
[10] Y. Zhang, B.-O. Guan, and H.-Y. Tam, "Ultra-short distributed Bragg reflector fiber laser for sensing applications," *Opt. Express*, vol. 17, no. 12, pp. 10050-10055, Jun. 2009.
[11] H. Renner, "Effective-index increase, form birefringence and transition losses in UV-side-illuminated photosensitive fibers," *Opt. Express*, vol. 9, no. 11, pp. 546-560, Nov. 2001.
[12] G. A. Ball, G. Meltz, and W. W. Morey, "Polarimetric heterodyning Bragg-grating fiber-laser sensor," *Opt. Lett.*, vol. 18, no. 22, pp. 1976-1978, Nov. 1993.
[13] L.-Y. Shao, X. Dong, A. P. Zhang, H.-Y. Tam, and S. He, "High-resolution strain and temperature sensor based on distributed Bragg reflector fiber laser," *IEEE Photonics Technol. Lett.*, vol. 19, no. 17-20, pp.

1598-1600, Sep.-Oct. 2007.
[14] L. Y. Shao, X. Y. Dong, and H. Y. Tam, "Fibre-optic load sensor based on polarimetric DBR fibre laser," *Electron. Lett.*, vol. 44, no. 2, Jan. 2008.
[15] W. Liu, T. Guo, A. C.-l. Wong, H.-Y. Tam, and S. He, "Highly sensitive bending sensor based on Er+-doped DBR fiber laser," *Opt. Express*, vol. 18, no. 17, pp. 17834-17840, Aug. 2010.
[16] B. O. Guan, H. Y. Tam, S. T. Lau, and H. L. W. Chan, "Ultrasonic hydrophone based on distributed Bragg reflector fiber laser," *IEEE Photonics Technol. Lett.*, vol. 17, no. 1, pp. 169-171, Jan. 2005.
[17] Y. Liang, H. Sun, L. Cheng, L. Jin, and B.-O. Guan, "High spatiotemporal resolution optoacoustic sensing with photothermally induced acoustic vibrations in optical fibres," *Nat. Commun.*, vol. 12, no. 1, Jul. 2021, Art. no. 4139.
[18] Y. Liang *et al.*, "Optical-resolution functional gastrointestinal photoacoustic endoscopy based on optical heterodyne detection of ultrasound," *Nat. Commun.*, vol. 13, no. 1, Dec. 2022, Art. no. 7604.
[19] Z. E. Harutjunian, W. H. Loh, R. I. Laming, and D. N. Payne, "Single polarisation twisted distributed feedback fibre laser," *Electron. Lett.*, vol. 32, no. 4, pp. 346-348, Feb. 1996.
[20] W. Fan, B. Chen, X. C. Li, L. R. Chen, and Z. Q. Lin, "Stress-induced single polarization DFB fiber lasers," *Opt. Commun.*, vol. 204, no. 1-6, pp. 157-161, Apr. 2002.
[21] S. Yamashita and G. J. Cowle, "Single-polarization operation of fiber distributed feedback (DFB) lasers by injection locking," *J. Lightwave Technol.*, vol. 17, no. 3, pp. 509-513, Mar. 1999.
[22] S. A. Babin, D. V. Churkin, A. E. Ismagulov, S. I. Kablukov, and M. A. Nikulin, "Single frequency single polarization DFB fiber laser," *Laser Phys. Lett.*, vol. 4, no. 6, pp. 428-432, Jun. 2007.
[23] J. L. Philipsen *et al.*, "Polarisation control of DFB fibre laser using UV-induced birefringent phase-shift," *Electron. Lett.*, vol. 34, no. 7, pp. 678-679, Apr. 1998.
[24] H. Wang *et al.*, "High temperature resistant ultra-short DBR Yb-doped fiber laser," *Appl. Optics*, vol. 58, no. 16, pp. 4474-4478, Jun. 2019.
[25] B.-O. Guan, Y. Zhang, H.-J. Wang, D. Chen, and H.-Y. Tam, "High-temperature-resistant distributed Bragg reflector fiber laser written in Er/Yb co-doped fiber," *Opt. Express*, vol. 16, no. 5, pp. 2958-2964, Mar. 2008.
[26] Z. Xu, P. Xiao, Y. Liang, L. Jin, Y. Ran, and B.-O. Guan, "Compact polarimetric heterodyning DBR fiber laser sensor with high temperature resistance," *Opt. Lett.*, vol. 46, no. 2, pp. 218-221, Jan. 2021.
[27] R. Chen *et al.*, "Regenerated distributed Bragg reflector fiber lasers for high-temperature operation," *Opt. Lett.*, vol. 38, no. 14, pp. 2490-2492, Jul. 2013.
[28] J. Canning, "Fibre gratings and devices for sensors and lasers," *Laser Photon. Rev.*, vol. 2, no. 4, pp. 275-289, Aug. 2008.
[29] M. H. Wang *et al.*, "Single-mode sapphire fiber Bragg grating," *Opt. Express*, vol. 30, no. 9, pp. 15482-15494, Apr. 2022.
[30] D. Grobnic, C. Hnatovsky, S. Dedyulin, R. B. Walker, H. M. Ding, and S. J. Mihailov, "Fiber Bragg Grating Wavelength Drift in Long-Term High Temperature Annealing," *Sensors*, vol. 21, no. 4, Feb. 2021, Art. no. 1454.
[31] P. Xuantung, J. Si, T. Chen, Z. Niu, and X. Hou, "Ultra-high-temperature resistant distributed Bragg reflector fiber laser based on type II-IR fiber Bragg gratings," *Appl. Optics*, vol. 59, no. 10, pp. 3081-3085, Apr. 2020.
[32] A. Martinez, M. Dubov, I. Khrushchev, and I. Bennion, "Direct writing of fibre Bragg gratings by femtosecond laser," *Electron. Lett.*, vol. 40, no. 19, pp. 1170-1172, Sep. 2004.
[33] A. Donko, M. Beresna, Y. Jung, J. Hayes, D. J. Richardson, and G. Brambilla, "Point-by-point femtosecond laser micro-processing of independent core-specific fiber Bragg gratings in a multi-core fiber," *Opt. Express*, vol. 26, no. 2, pp. 2039-2044, Jan. 2018.
[34] Y. Lai, A. Martinez, I. Khrushchev, and I. Bennion, "Distributed Bragg reflector fiber laser fabricated by femtosecond laser inscription," *Opt. Lett.*, vol. 31, no. 11, pp. 1672-1674, Jun. 2006.
[35] J. Thomas, C. Voigtlaender, R. G. Becker, D. Richter, A. Tuennermann, and S. Nolte, "Femtosecond pulse written fiber gratings: a new avenue to integrated fiber technology," *Laser Photon. Rev.*, vol. 6, no. 6, pp. 709-723, Nov. 2012.
[36] R. J. Williams, N. Jovanovic, G. D. Marshall, G. N. Smith, M. J. Steel, and M. J. Withford, "Optimizing the net reflectivity of point-by-point fiber Bragg gratings: the role of scattering loss," *Opt. Express*, vol. 20, no. 12, pp. 13451-13456, Jun. 2012.
[37] M. Ams, P. Dekker, S. Gross, and M. J. Withford, "Fabricating waveguide Bragg gratings (WBGs) in bulk materials using ultrashort laser pulses," *Nanophotonics*, vol. 6, no. 5, pp. 743-763, Sep. 2017.
[38] P. Lu *et al.*, "Plane-by-Plane Inscription of Grating Structures in Optical Fibers," *J. Lightwave Technol.*, vol. 36, no. 4, pp. 926-931, Feb. 2018.
[39] G. Zhang, G. Cheng, M. Bhuyan, C. D'Amico, and R. Stoian, "Efficient point-by-point Bragg gratings fabricated in embedded laser-written silica waveguides using ultrafast Bessel beams," *Opt. Lett.*, vol. 43, no. 9, pp. 2161-2164, May 2018.
[40] K. M. Aghdami, A. Rahnama, E. Ertorer, and P. R. Herman, "Laser nano-filament explosion for enabling open-grating sensing in optical fibre," *Nat. Commun.*, vol. 12, no. 1, Nov. 2021, Art. no. 6344.
[41] E. Ertorer, M. Haque, J. Z. Li, and P. R. Herman, "Femtosecond laser filaments for rapid and flexible writing of fiber Bragg grating," *Opt. Express*, vol. 26, no. 7, pp. 9323-9331, Apr. 2018.
[42] X. Xu *et al.*, "Slit Beam Shaping for Femtosecond Laser Point-by-Point Inscription of High-Quality Fiber Bragg Gratings," *J. Lightwave Technol.*, vol. 39, no. 15, pp. 5142-5148, Aug. 2021.
[43] Y. Cheng *et al.*, "Control of the cross-sectional shape of a hollow microchannel embedded in photostructurable glass by use of a femtosecond laser," *Opt. Lett.*, vol. 28, no. 1, pp. 55-57, Jan. 2003.
[44] N. Jovanovic *et al.*, "Polarization-dependent effects in point-by-point fiber Bragg gratings enable simple, linearly polarized fiber lasers," *Opt. Express*, vol. 17, no. 8, pp. 6082-6095, Apr. 2009.
[45] J. He *et al.*, "Slit Beam Shaping for Femtosecond Laser Point-by-Point Inscription of Highly Localized Fiber Bragg Grating," *J. Lightwave Technol.*, vol. 40, no. 16, pp. 5722-5728, Aug. 2022.
[46] E. Ronnekleiv, M. N. Zervas, and J. T. Kringlebotn, "Modeling of polarization-mode competition in fiber DFB lasers," *IEEE J. Quantum Electron.*, vol. 34, no. 9, pp. 1559-1569, Sep. 1998.
[47] M. I. Skvortsov, A. A. Wolf, A. V. Dostovalov, A. A. Vlasov, V. A. Akulov, and S. A. Babin, "Distributed feedback fiber laser based on a fiber Bragg grating inscribed using the femtosecond point-by-point technique," *Laser Phys. Lett.*, vol. 15, no. 3, Mar. 2018, Art. no. 035103.
[48] C. D. Butter and G. B. Hocker, "Fiber optics strain gauge," *Appl. Optics*, vol. 17, no. 18, pp. 2867-2869, Jul. 1978.
[49] K. P. Koo and A. D. Kersey, "Fibre laser sensor with ultrahigh strain resolution using interferometric interrogation," *Electron. Lett.*, vol. 31, no. 14, pp. 1180-1182, Jul. 1995.
[50] M. Ams, G. D. Marshall, D. J. Spence, and M. J. Withford, "Slit beam shaping method for femtosecond laser direct-write fabrication of symmetric waveguides in bulk glasses," *Opt. Express*, vol. 13, no. 15, pp. 5676-5681, Jul. 2005.
[51] J. Wang, G. M. H. Flockhart, and D. Uftamchandanie, "Demodulation of Polarimetric Fiber Laser Ultrasonic Sensor With Intensity Noise Cancellation," *J. Lightwave Technol.*, vol. 37, no. 18, pp. 4872-4880, Sep. 2019.
[52] L. Zhong, Y. Wang, D. Tan, and J. Qiu, "Toward 3D Integration of Highly See-Through Photonic Circuits in Glass," *Laser Photon. Rev.*, vol. 17, no. 6, Jun. 2023.
[53] K. Guo *et al.*, "Beat frequency tuning in dual-polarization distributed feedback fiber laser using side polishing technique," *Opt. Express*, vol. 26, no. 26, pp. 34699-34710, Dec. 2018.
[54] X. Bai, Q. Sheng, H. Zhang, S. Fu, W. Shi, and J. Yao, "Influence of seed power and gain fiber temperature on output linewidth in single-frequency EYDFA," *Infrared and Laser engineering*, vol. 47, no. 10, pp. 109-114, Oct. 2018.
[55] M. J. O'Dwyer, C. C. Ye, S. W. James, and R. P. Tatam, "Thermal dependence of the strain response of optical fibre Bragg gratings," *Meas. Sci. Technol.*, vol. 15, no. 8, pp. 1607-1613, Aug. 2004.
[56] C. Hu, Z. Yu, and A. Wang, "All fiber-optic multi-parameter structure health monitoring system," *Opt. Express*, vol. 24, no. 18, pp. 20287-20296, Sep. 2016.
[57] J. He, C. Hu, D. Hu, and A. Wang, "High-temperature all-fiber non-destructive multi-parameter sensing system with consistent performance," *Opt. Lett.*, vol. 45, no. 7, pp. 1722-1725, Apr. 2020.
[58] B.-O. Guan, L. Jin, L. Cheng, and Y. Liang, "Acoustic and Ultrasonic Detection With Radio-Frequency Encoded Fiber Laser Sensors," *IEEE J. Sel. Top. Quantum Electron.*, vol. 23, no. 2, Mar.-Apr. 2017, Art. no. 5601712.
[59] X. Lin, Y. Liang, L. Jin, and L. Wang, "Dual-Polarized Fiber Laser Sensor for Photoacoustic Microscopy," *Sensors*, vol. 19, no. 21, Nov. 2019.
[60] A. D. W. McKie, J. W. Wagner, J. B. Spicer, and J. B. Deaton, "Dual-beam interferometer for the accurate determination of surface-wave velocity," *Appl. Optics*, vol. 30, no. 28, pp. 4034-4039, Oct. 1991.

Runxiao Chen was born in Guangdong, China, in 1998. He received the B.S. degree in College of Physics and Optoelectronic Engineering from Shenzhen University, Shenzhen, China, in 2020. He is now working toward the Ph.D. degree in Shenzhen University. His current research interests focus on femtosecond laser micromachining, fiber lasers, and optical fiber sensors.

Xizhen Xu was born in Guangdong, China, in 1990. He received the B.S. degree from the College of Science, Zhejiang University of Technology, Hangzhou, China, in 2013, and the M.S. degree and Ph.D. degree in optical engineering from Shenzhen University, Shenzhen, China, in 2016 and 2019. From 2019 to 2021, he was with Shenzhen University, Shenzhen, China, as a Postdoctoral Research Fellow. He is currently with Shenzhen University, Shenzhen, China, as an Assistant Professor. His current research interests include femtosecond laser micromachining, optical fiber sensors, and fiber Bragg gratings. He has authored or coauthored 3 patent applications and more than 50 journal and conference papers.

Kuikui Guo was born in Henan, China, in 1988. He received the B.S. degree from the Institute of Photoelectric Information, Changchun University of Science and Technology, Changchun, China, in 2013, and the Ph.D. degree in optical engineering from Shenzhen University, Shenzhen, China, in 2020. From 2020 to 2022, he has been a Postdoctoral Researcher with the Guangdong and Hong Kong Joint Research Centre for Optical Fiber Sensors, Shenzhen University. Since 2022, he has been an Assistant Professor in Dongguan University of Technology. His research interests include optical fiber laser sensors and fiber Bragg gratings.

Yihang Wang was born in Hebei, China, in 2002. He received the B.Eng. degree in College of Physics and Optoelectronic Engineering from Shenzhen University, Shenzhen, China, in 2023. He is now working toward the M.S. degree in Shenzhen University. His current research interests focus on distributed optical fiber sensing and signal processing.

Bin Du was born in Henan, China, in 1992. He received the B.S. degree in flight vehicle propulsion engineering from the School of Astronautics, Beihang University, Beijing, China, in 2016, and the Ph.D. degree in optical engineering from Shenzhen University, Shenzhen, China, in 2021. From 2021 to 2023, he has been a Postdoctoral Researcher with the Guangdong and Hong Kong Joint Research Centre for Optical Fiber Sensors, Shenzhen University. Since 2023, he has been an Assistant Professor in Shenzhen University. His current research interests include distributed optical fiber sensing technology, vibration sensor, and gas sensor.

Feng Zhu received the Ph.D. degree in optical engineering from Shenzhen University, Shenzhen, China, in 2022. Since 2022, has been a Postdoctoral Researcher in Shenzhen University. His current research interests include fiber lasers and low-dimensional materials.

Ying Wang was born in Henan, China, in 1983. He received the B.S. degree in applied physics and the Ph.D. degree in physical electronics from the Huazhong University of Science and Technology, Wuhan, China, in 2004 and 2010, respectively. From 2010 to 2011, he worked with the Department of Electrical Engineering, Hong Kong Polytechnic University, Hong Kong, as a Research Associate. And from 2011 to 2015, he worked with the School of Science, Wuhan Institute of Technology, Wuhan, China. Since 2015, he has been with the College of Physics and Optoelectronic Engineering, Shenzhen University, Shenzhen, China, as an Associate Professor. His research interests include optical fiber sensors, photonic crystal fibers and devices, and femtosecond laser micromachining.

Changrui Liao (Member, IEEE) received the B.Eng. degree in optical engineering and the M.S. degree in physical electronics from the Huazhong University of Science and Technology, Wuhan, China, in 2005 and 2007, respectively, and the Ph.D. degree in electrical engineering from Hong Kong Polytechnic University, Hong Kong, in 2012. Since 2013, he has been in Shenzhen University, Shenzhen, China, as an Assistant Professor/Associate /Professor/Distinguished Professor. His current research interests include femtosecond laser micromachining, optical fiber sensors, biosensing and opto-microfluidics.

Yiping Wang (Fellow, OSA/Senior Member, IEEE) was born in Chongqing, China, in 1971. He received the B.Eng. degree in precision instrument engineering from Xi'an Institute of Technology, China, in 1995 and the M.S. degree and Ph.D. degree in optical engineering from Chongqing University, China, in 2000 and 2003, respectively. From 2003 to 2005, he was with Shanghai Jiao Tong University, China, as a Postdoctoral Fellow. From 2005 to 2007, he was with the Hong Kong Polytechnic University, as a Postdoctoral Fellow. From 2007 to 2009, he was with the Institute of Photonic Technology (IPHT), Jena, Germany, as a Humboldt Research Fellow. From 2009 to 2011, he was with the Optoelectronics Research Centre (ORC), University of Southampton, U.K., as a Marie Curie Fellow. Since 2012, he has been with Shenzhen University, Shenzhen, China, as a Distinguished Professor. His current research interests focus on optical fiber sensors, fiber gratings, and photonic crystal fibers. He has authored or coauthored 1 book, 25 patent applications, and more than 420 journal and conference papers. Prof. Wang is a Senior Member of IEEE, the Optical Society of America, and the Chinese Optical Society.

Jun He (Member, IEEE) was born in Hubei, China, in 1985. He received the B.Eng. degree in electronic science and technology from Wuhan University, Wuhan, China, in 2006 and the Ph.D. degree in electrical engineering from the Institute of Semiconductors, Chinese Academy of Sciences (CAS), Beijing, China, in 2011. From 2011 to 2013, he was with Huawei Technologies, Shenzhen, China, as a Research Engineer. From 2013 to 2015, he was with Shenzhen University, Shenzhen, China, as a Postdoctoral Research Fellow. From 2015 to 2016, he was with The University of New South Wales (UNSW), Sydney, Australia, as a Visiting Fellow. Since 2017, he has been in Shenzhen University, Shenzhen, China, as an Assistant Professor/ Associate Professor/Distinguished Professor. His current research interests focus on optical fiber sensors, fiber Bragg gratings (FBGs), and fiber lasers. He has authored or coauthored 8 patent applications and more than 90 journal and conference papers. Dr. He is a member of the Optical Society of America.